Received: 16 March 2022 | Revised: 17 April 2022 | Accepted: 7 May 2022

DOI: 10.1002/rcs.2416

ORIGINAL ARTICLE

The International Journal of Medical Robotics and Computer Assisted Surgery

WILEY

The stability investigation of variable viscosity control in the human-robot interaction

Lin Dong | Nicolas Perrin | Florian Richer | Agnes Roby-Brami | Guillaume Morel

[1]Institut des Systèmes Intelligents et de Robotique, Sorbonne Universités UPMC Univ. Paris 06, Paris, France

Correspondence
Guillaume Morel, Institut des Systèmes Intelligents et de Robotique, Sorbonne Universités UPMC Univ. Paris 06, UMR 7222, Paris, 75005, France.
Email: morel@isir.upmc.fr

Present address
Lin Dong, Center on Frontiers of Computing Studies, Peking University, Beijing, ?00089, China.

Funding information
French FUI, Grant/Award Number: ANR-11-LABX-0004

Abstract

Background: For many co-manipulative applications, variable damping is a valuable feature provided by robots. One approach is implementing a high viscosity at low velocities and a low viscosity at high velocities. This, however, is proven to have the possibility to alter human natural motion performance.

Methods: We show that the distortion is caused by the viscosity drop resulting in robot's resistance to motion. To address this, a method for stably achieving the desired behaviour is presented. It involves leveraging a first-order linear filter to slow the viscosity variation down.

Results: The proposition is supported by a theoretical analysis using a robotic model. Meanwhile, the user performance in human-robot experiments gets significantly improved, showing the practical efficiency in real applications.

Conclusions: This paper discusses the variable viscosity control in the context of co-manipulation. An instability problem and its solution were theoretically shown and experimentally evidenced through human-robot experiments.

KEYWORDS
co-manipulation, HRI, human-robot interaction, impedance control, stability, viscosity control

1 | INTRODUCTION

Co-manipulation is a paradigm in which a robot and a person manipulate an object or a tool at the same time.[1–3] The co-manipulation combines the advantages of human operators, such as quick learning and adaptability,[4,5] with the advantages of robots, such as the capacity to improve precision and do repetitive jobs without tiring.[6] Therefore, nowadays, the concept of co-manipulation is applied to many tasks so as to optimise ergonomics and to enhance gesture quality.[7–9] For example, in a human-robot co-manipulation sawing task,[10] the authors leverage a myoelectric feedback interface to online estimate human muscle fatigue level and then control the robot to adapt its physical behaviour to the human motor fatigue with the learnt task execution skill. The authors in[11] proposes a real-time model-based reinforcement learning impedance controller to assist human operators in a collaborative lifting task by online optimising the stiffness and damping impedance control parameters to minimise the human effort. The authors in[12] demonstrate that a collaborative industrial robot with active compliance controller works with a human operator to disassemble the press-fitted components of an automotive water pump.

Impedance control is a standard paradigm for controlling a co-manipulator in a co-manipulative task.[13,14] While elastic fields (stiffness) are used for guidance through virtual fixtures, viscous

fields provide appropriate damping or tremor filtering.[15] Furthermore, a co-manipulator may vary its impedance during manipulation activities to give adaptive assistance to changing operating circumstances.

This method was first presented in[16] for assisting point-to-point movements. It is based upon the experimental finding that when a human operator collaborates with another one to transport an object along a linear path, the operator's arm viscosity decreases at a rapid rate. A robot controller is implemented to imitate this behaviour based on the above-mentioned observation: the viscosity is set large for low velocities while it is set a small value after the velocity reaches the threshold. Consequently, human-robot co-manipulative tasks have been demonstrated to follow similar trajectories as in human-human co-manipulative tasks. According to the authors in,[17] this controller is then updated to be "optimal", that is, the value of viscosity coefficient is an exponential function with respect to time once the threshold is achieved. The resulting velocity profiles of collaborative point-to-point motions have the bell shape of minimal jerk trajectories, which, according to the authors, indicates that the movements are "natural".[18] Meanwhile, the same experiment conducted using an abrupt change of viscosity, as proposed in,[16] induces degraded control performance during point-to-point movements. This suggests that the way the viscosity variation is dynamically programed impacts the coupled dynamics.

The variable viscosity method is also used for more advanced tasks. In,[19] an intention-driven controller is proposed for compliantly-driven robots and tested on a lower-limb exoskeleton. The damping coefficient of the controller is online adjusted with the adaptation of the human motion intention through weighting function to suit human behaviour for better collaboration. In a manual welding task with robot assistance,[20] the damping coefficient is designed to be a piece-wise linear function of the robot velocity norm. Given the reported performance improvement, as well as the simplicity of the implementation, this controller is used as a starting point of our research.

Our investigation concerns the dynamic behaviour of the couple user + co-manipulator. In particular, we are interested in the stabilisation of a movement at a given desired velocity. In Section 2.1, we first study this question from a theoretical perspective, within a robotics framework. To this aim, we study the coupling between a conventional velocity controlled robot and the co-manipulator driven by the controller proposed in.[20] We show that, under certain conditions, the coupling may exhibit unstable behaviour. In Section 2.2, we propose a solution to stabilise the coupled behaviour. It consists in introducing a secondary linear dynamics to slow down the viscosity coefficient time variations. To complement the theoretical analysis, in Section 3.1, we conduct experiments with human subjects trying to regulate their hand velocity while connected to a co-manipulator equipped with the variable viscosity controller. We observe oscillatory behaviours when the unstable conditions of the robotics-based analysis are encountered. Then the human experiments in Section 3.2 (reproducing those of Section 3.1) validate the effectiveness of the proposed method.

2 | MATERIALS AND METHODS

2.1 | Variable viscosity coefficient

2.1.1 | Basic control law

This paper is part of a research aimed to study co-manipulation for minimally invasive surgery. Different from tele-surgery, the surgeon and the co-manipulator together hold and maneuver the instrument during the operation. We consider a co-manipulative robot named Achilles[21] programed to assist a human subject. Achilles is a light-weight robot fabricated by Haption company, France, see its sketch in Figure 3. It has 6 revolute joints: first three are actuated and last three are passive. The last three joints intersect at a point P, thus forming a spherical passive wrist with P as the wrist centre.

When the human subject moves his/her hand, the robotic device desired behaviour consists in exhibiting:

- a high viscosity for low hand velocities, in the aim of smoothing fine gestures;
- a low viscosity at high velocities, in the aim of limiting the viscous resisting force during large and low precision movements imposed by the user.

The user holds a handle connected to the end-effector through the passive spherical wrist centred at point P. The device control input is a force $\mathbf{f} \in \mathbb{R}^3$ exerted at point P. Its outputs consist in position $\mathbf{x} \in \mathbb{R}^3$ and velocity $\mathbf{v} \in \mathbb{R}^3$ of P, obtained from the robot sensors and used as system outputs.

With such a device, we can programme a viscosity controller as:

$$\mathbf{f} = -b\mathbf{v} \,. \tag{1}$$

A variable viscosity control can be implemented by computing the viscosity coefficient $b \in \mathbb{R}$ as a direct function (static map) of the norm of the velocity:

$$b = b_{\max} \cdot \lambda(\|\mathbf{v}\|), \tag{2}$$

with $b_{\max}$ the maximal viscosity and $0 \leq \lambda \leq 1$.

A simple implementation, proposed in,[20] consists in linearly interpolating the viscosity coefficient between two values, $b_{\min}$ and $b_{\max}$, with $0 < b_{\min} < b_{\max}$:

$$\lambda = \begin{cases} 1, \text{ if } \|\mathbf{v}\| < v_{\min}, \\ \dfrac{b_{\min}}{b_{\max}}, \text{ if } \|\mathbf{v}\| > v_{\max}, \\ 1 - \dfrac{\|\mathbf{v}\| - v_{\min}}{v_{\max} - v_{\min}} \left(1 - \dfrac{b_{\min}}{b_{\max}}\right), \text{ otherwise.} \end{cases} \tag{3}$$

Figure 1 shows the variation of b as a function of $\|\mathbf{v}\|$.

This approach has a major issue: within a particular range of velocities, the robot-exerted resistive force exhibits a decreasing function of the velocity amplitude, as shown in Figure 2. This

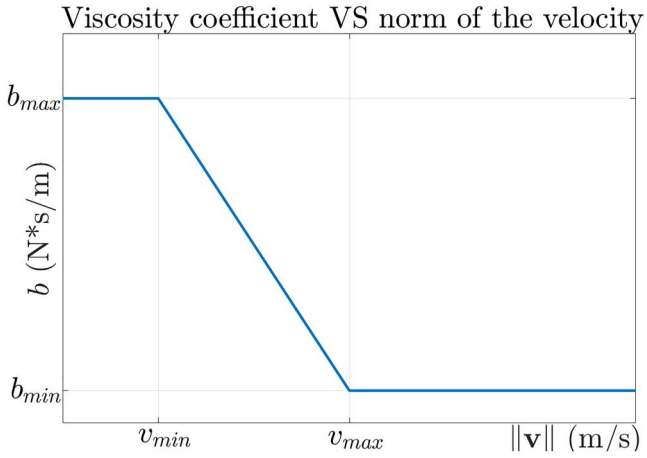

FIGURE 1 The relation of viscosity coefficient and velocity norm

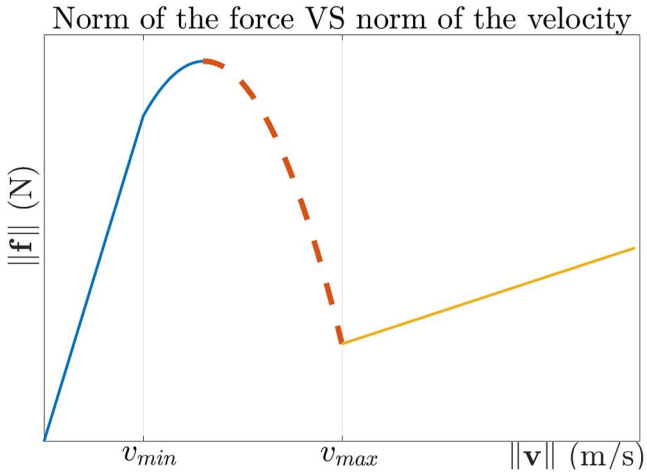

FIGURE 2 The relation of force norm and velocity norm

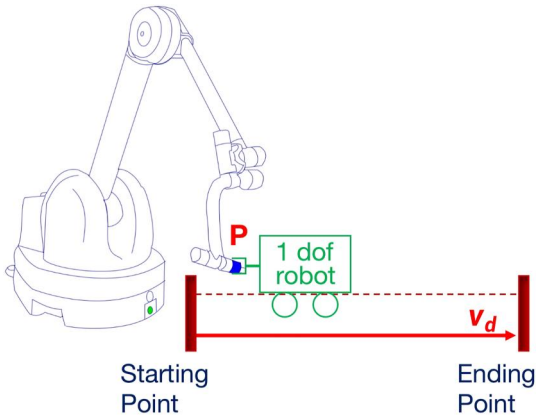

FIGURE 3 The conceptual illustration of the designed task for instability analysis

phenomenon is similar to the Stribeck effect, which is used in tribology to explain the decrease of friction force between the static and dynamic regimes. Taken as a local positive feedback, this behaviour can cause instability at low velocities, leading to stick-slip movements.[22] Analogously, we may anticipate the system to have unstable behaviour when the user attempts to maneuver the robot at a velocity that is in the negative slope area (illustrated as dashed red curve in Figure 2).

2.1.2 | Theoretical analysis of instability within a robotics framework

We first evaluate the proposed control law from a theoretical perspective. Consider such a task: a 1 dof control robot connects Achilles at its wrist centre point *P* and guides Achilles to move from a given starting point to a given ending point. The movement is supposed to keep a straight line path at constant velocity v_d. Achilles, the co-manipulator, acts as the follower and is controlled according to Equations (1)–(3). Figure 3 is an conceptual illustration of the task.

The designed task is a simplified version for theoretical analysis of the practical experiment where a human subject is involved (the experiment detail is provided in Section 3). There are no consensual models available in the literature to precisely depict the complex human dynamic behaviour. Therefore, considering the task requirement of keeping at constant velocity when following a given line, we assume that the assistive control robot exploits a standard PI velocity controller:

$$f_c = k_p(v_d - v) + k_i \int (v_d - v)dt, \tag{4}$$

where f_c is the force exerted by the assistive robot, k_p (resp. k_i) is the proportional (resp. integral) velocity controller gain. We model the end-effector of the assistive robot as a pure mass *m* which is affected by the co-manipulator force *f* as well as the command force f_c, and we write its closed loop behaviour as:

$$m\dot{v} = f + f_c = -bv + k_p(v_d - v) + k_i \int (v_d - v)dt\ . \tag{5}$$

To keep things simple, we'll use the following system state variables:

$$x_1 = \int (v_d - v)dt, \tag{6}$$

$$x_2 = v_d - v\ . \tag{7}$$

Their derivatives are consequently obtained as:

$$\dot{x_1} = x_2, \tag{8}$$

$$\dot{x_2} = -\dot{v}\ . \tag{9}$$

We now limit the study around an equilibrium point, where *b* can be written as linear function of *v*:

$$b = b_0 - \alpha v\ . \tag{10}$$

α is the viscosity slope and b_0 is where the function intersects with the viscosity axis.

According to Equation (7), $v = v_d - x_2$. Then Equation (5) becomes:

$$\dot{v} = \frac{k_i}{m}x_1 + \frac{k_p + b_0 - 2\alpha v_d}{m}x_2 + \frac{\alpha}{m}x_2^2 + \frac{\alpha v_d^2 - b_0 v_d}{m} . \tag{11}$$

Combining Equations (6)–(11), we obtain the system closed-loop state space equations:

$$\begin{pmatrix} \dot{x_1} \\ \dot{x_2} \end{pmatrix} = \begin{pmatrix} x_2 \\ -\frac{k_i}{m}x_1 - \frac{k_p + b_0 - 2\alpha v_d}{m}x_2 - \frac{\alpha}{m}x_2^2 - \frac{\alpha v_d^2 - b_0 v_d}{m} \end{pmatrix} . \tag{12}$$

Linearising around the equilibrium point $v = v_d$ (corresponding to $(x_1, x_2) = (0, 0)$), one gets:

$$\begin{pmatrix} \dot{x_1} \\ \dot{x_2} \end{pmatrix} = \underbrace{\begin{pmatrix} 0 & 1 \\ -\frac{k_i}{m} & -\frac{k_p + b_0 - 2\alpha v_d}{m} \end{pmatrix}}_{=:\mathbf{A}(v_d)} \begin{pmatrix} x_1 \\ x_2 \end{pmatrix} . \tag{13}$$

The eigenvalues of $\mathbf{A}(v_d)$ are:

$$e_{1,2} = \frac{-T \pm \sqrt{T^2 - 4k_i m}}{2m}, \tag{14}$$

with $T = k_p + b_0 - 2\alpha v_d$. Since $m > 0$, the real parts of $e_{1,2}$ are both negative iff

$$\alpha < \frac{b_0 + k_p}{2v_d}. \tag{15}$$

We hence draw a conclusion that in a local region the system is asymptotically stable iff $\alpha < (b_0 + k_p)/(2v_d)$. If $\alpha \geq (b_0 + k_p)/(2v_d)$, the equilibrium becomes unstable. For the above velocity control task, the stability condition is described as: when a variable viscosity coefficient with slope α is given, to keep the velocity at v_d, the stiffness k_p must be high enough to ensure the system locally stable.

2.2 | Our proposition to the instability problem

2.2.1 | Slowing down viscosity variation by adding a dynamics

In order to solve this instability problem, we apply to the viscosity coefficient a first-order low pass filter which is therefore named as viscosity coefficient filter. The purpose of adding this filter is to decelerate the viscosity coefficient variation. This further slows down the viscous force variation, giving the users more time to adjust themselves. Thus the control law writes:

$$\mathbf{f} = -b_f \mathbf{v}, \tag{16}$$

with b_f defined as the filtered viscosity coefficient by equation:

$$\dot{b_f} = \frac{b - b_f}{\tau}, \tag{17}$$

where τ is the filter time constant (unit: second), b being obtained from the static velocity-viscosity map used in the previous section.

2.2.2 | Theoretical investigation of stability in a robot-robot configuration

We use the same model established in Section 2.1.2 for the theoretical investigation. Now the system dynamics becomes:

$$m\dot{v} = -b_f v + k_p(v_d - v) + k_i \int (v_d - v)dt . \tag{18}$$

Keeping x_1 and x_2 the same as in Equations (6) and (7), we select x_3 as:

$$x_3 = b_d - b_f . \tag{19}$$

whose derivative is (recall that $b = b_0 - \alpha v$, therefore, $b_d := b(v_d)$):

$$\dot{x_3} = -\dot{b_f} \tag{20}$$

$$= \frac{1}{\tau}(b_f - b_0 + \alpha v)$$

$$= \frac{1}{\tau}(b_f - b_0 + \alpha(v_d - x_2)) \tag{21}$$

$$= -\frac{\alpha}{\tau}x_2 - \frac{1}{\tau}x_3 + \frac{\alpha v_d + b_d - b_0}{\tau} .$$

The closed loop dynamics now writes:

$$m\dot{v} = -(b_d - x_3)(v_d - x_2) + k_p x_2 + k_i x_1, \tag{22}$$

then the derivative of x_2 is:

$$\dot{x_2} = -\dot{v} = -\frac{k_i}{m}x_1 - \frac{k_p + b_d}{m}x_2 - \frac{v_d}{m}x_3 + \frac{1}{m}x_2 x_3 + \frac{b_d v_d}{m} . \tag{23}$$

Equations (8), (21) and (23) together deduce the new state space equations:

$$\begin{pmatrix} \dot{x_1} \\ \dot{x_2} \\ \dot{x_3} \end{pmatrix} = \begin{pmatrix} x_2 \\ -\frac{k_i}{m}x_1 - \frac{k_p + b_d}{m}x_2 - \frac{v_d}{m}x_3 + \frac{1}{m}x_2 x_3 + \frac{b_d v_d}{m} \\ -\frac{\alpha}{\tau}x_2 - \frac{1}{\tau}x_3 + \frac{\alpha v_d + b_d - b_0}{\tau} \end{pmatrix} . \tag{24}$$

At the equilibrium point, we do the Jacobian linearisation:

$$\begin{pmatrix} \dot{x_1} \\ \dot{x_2} \\ \dot{x_3} \end{pmatrix} = \underbrace{\begin{pmatrix} 0 & 1 & 0 \\ -\frac{k_i}{m} & -\frac{k_p + b_d}{m} + \frac{1}{m}x_3 & -\frac{v_d}{m} + \frac{1}{m}x_2 \\ 0 & -\frac{\alpha}{\tau} & -\frac{1}{\tau} \end{pmatrix}}_{=:\mathbf{B}(v)} \begin{pmatrix} x_1 \\ x_2 \\ x_3 \end{pmatrix} . \tag{25}$$

At the reference velocity of the PI control, the viscosity achieves the desired value. To put it another way, when $v = v_d$, we have $b_f = b_d$. Thus, the system equilibrium point is $(x_1, x_2, x_3) = (0, 0, 0)$, and around this point Equation (25) rewrites as:

$$\begin{pmatrix} \dot{x_1} \\ \dot{x_2} \\ \dot{x_3} \end{pmatrix} = \underbrace{\begin{pmatrix} 0 & 1 & 0 \\ -\frac{k_i}{m} & -\frac{k_p + b_d}{m} & -\frac{v_d}{m} \\ 0 & -\alpha\omega & -\omega \end{pmatrix}}_{=:\mathbf{B}(\omega)} \begin{pmatrix} x_1 \\ x_2 \\ x_3 \end{pmatrix} . \tag{26}$$

where $\omega = 1/\tau$, denotes the first-order low pass filter frequency.

We do not write down the eigenvalues of $\mathbf{B}(\omega)$ since they are too complex to fit here. Instead, we can prove the existence of a neighbourhood around zero for ω, for any given (positive) parameters, which ensures that all the eigenvalues of $\mathbf{B}(\omega)$ have negative real parts. We write out the characteristic polynomial of $\mathbf{B}(\omega)$:

$$\kappa^3 + \left(\frac{b_d + k_p}{m} + \omega\right)\kappa^2 + \left(\frac{b_d + k_p - \alpha v_d}{m}\omega + \frac{k_i}{m}\right)\kappa + \frac{k_i}{m}\omega .$$

When $\omega = 0$, the roots are $\kappa_{1,2}(0) = -\frac{b_d+k_p}{2m} \pm \sqrt{\left(\frac{b_d+k_p}{2m}\right)^2 - \frac{k_i}{m}}$, which have negative real parts and $\kappa_3(0) = 0$.

Eigenvalues as continuous functions of matrix coefficients, for small enough and positive ω, $\kappa_{1,2}(\omega)$ are converted into eigenvalues with negative real parts. $\kappa_3(\omega)$, on the other hand, is a real root of the following reformulated characteristic polynomial:

$$\kappa^3 + a\kappa^2 + b\kappa + c .$$

For small enough and positive ω, we can easily verify that a, b and c are all positive, since $\frac{b_d+k_p}{m} > 0$, and $\frac{k_i}{m} > 0$. If $\kappa \geq 0$, the characteristic polynomial is certainly not zero. The third eigenvalue is hence guaranteed to be strictly negative.

Eventually we can draw the conclusion that for small enough and positive ω, all the eigenvalues of $\mathbf{B}(\omega)$ consist of a negative real part. That is to say, regardless of the controller tuning, as long as τ is large enough (*i.e.*, variation of b_f slow enough), the system is locally asymptotically stable.

3 | EXPERIMENT RESULTS AND DISCUSSION

3.1 | Practical analysis of instability through human-comanipulator coupled experiments

We conducted experiments to evaluate whether the robot-robot theoretical instability evidenced in Section 2.1.2 could be observed in a human-robot configuration. An experimental scene was demonstrated in Figure 4.

Achilles' control input is a pure force at point P and therefore it can be easily fitted with the variable viscosity controller given by Equations (1)–(3).

For the experimental task a human user replaces the command robot and holds the handle of Achilles. The user is asked to move from the initial point to the final point materialised in the workspace. The distance between the two points is 0.4 m.

The user is asked to move the robot following a straight line between the starting and ending points while at the same time concentrating on the velocity. This is assisted by an interface illustrated in Figure 5, where a gauge provides the user a visual feedback of the current velocity norm. Concretely, the user is asked to keep the velocity at a constant desired value v_d during the movement, indicated by the black bold line in the graph.

As depicted in Figure 6, three velocity-to-viscosity static maps $\lambda(\|\mathbf{v}\|)$ are used to obtain three different experimental conditions, with a same value of v_d.

For Condition C_1, $\lambda(\|\mathbf{v}\|)$ is specially devised to ensure v_d falls inside the high viscosity coefficient area. For C_2, $\lambda(\|\mathbf{v}\|)$ is devised to ensure v_d falls inside the viscosity coefficient drop area. For C_3, $\lambda(\|\mathbf{v}\|)$ is devised to ensure v_d falls inside the low viscosity coefficient area. Notice that, according to the theoretical analysis, if a PI controlled robot was connected to the comanipulator, then stability

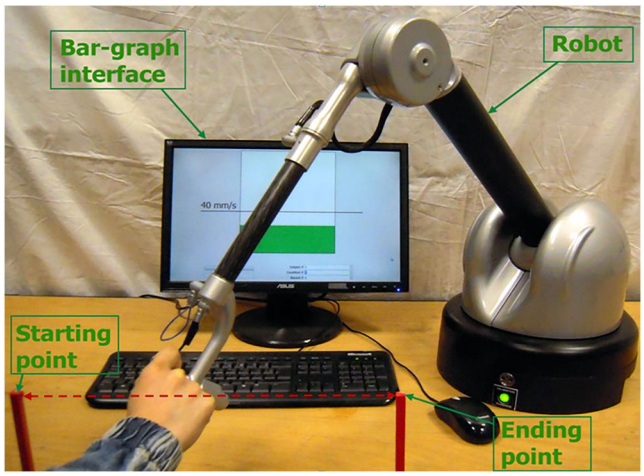

FIGURE 4 Experimental scene

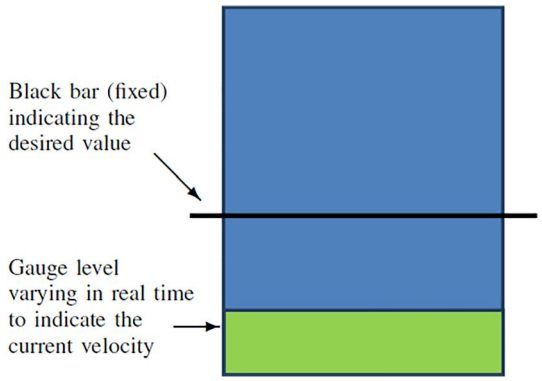

FIGURE 5 A gauge used to provide the user a visual velocity feedback

would be obtained for both C_1 and C_3 (since $\alpha = 0$) while, depending on the control parameters, instability could be observed for C_2.

Ten naive subjects, all right-handed, participated in the experiment. Conditions are randomly loaded. Before the formal recording, subjects were suggested to take a few trials for every condition so as to get familiar with the required force level for moving Achilles at v_d.

Figure 7 shows the typical behaviour of a random subject. From the figure, we see that the subject is able to maintain the velocity stable under C_1 and C_3. Further, the high viscosity coefficient under C_1 provides higher damping, leading to less error. The more important phenomenon is the instability observed under C_2: To reach v_d, the subject accelerates when initially at low velocity. The velocity acceleration corresponds to the viscosity drop, leading to a decreasing resistance to robot motion. The acceleration is easily getting higher than the subject's expectation, landing to the high velocity region (with $b = b_{\min}$). The subject then adjusts the velocity to slow down, but again than expected, too much deceleration lands to the low velocity region. The final result is that the subject fails to stabilise the velocity at v_d. The oscillation between two limit regions resembles the stick-slip motions observed in.[22]

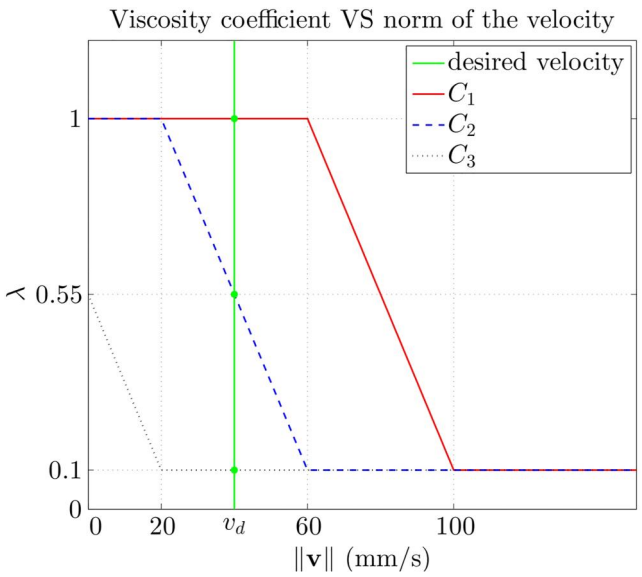

FIGURE 6 Three designs of $\lambda(\|\mathbf{v}\|)$. The three experiments share the same desired velocity v_d and the dropping slope

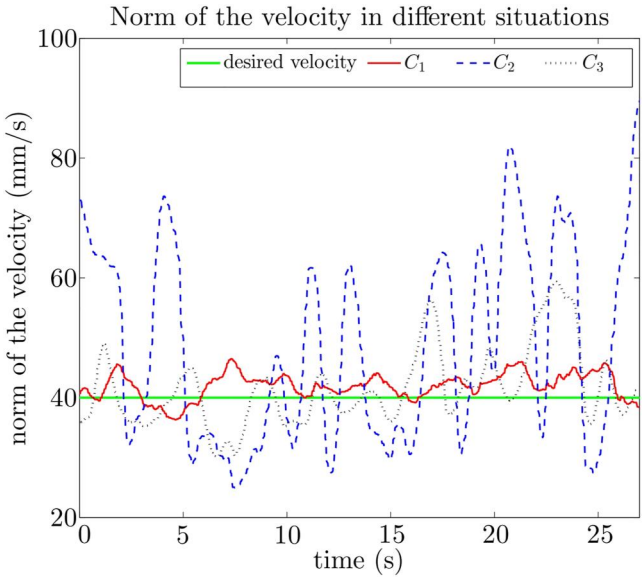

FIGURE 7 The velocity performance of a random subject under Conditions $C_1 - C_3$

This observation is typical for all subjects. Figure 8 is the Root-mean-square (RMS) of velocity errors and the corresponding standard deviations under the 3 conditions. To be more informative, the error of each subject is depicted with a small red dot.

We also conducted a Student's t-test for a quantitative assessment of the performance under $C_1 - C_3$. The RMS error under C_3 ($\mu = 4.7$, $\sigma = 0.94$, unit: mm/s, hereinafter the same) is more than twice compared with that under C_1 ($\mu = 2.2$, $\sigma = 0.57$), with a statistically significant difference ($p = 2.7 \times 10^{-6} \ll 0.05$). On the contrary, the RMS error under C_2 ($\mu = 13$, $\sigma = 3.5$) is almost three times of that under C_3, and the p-value ($p = 4.0 \times 10^{-5}$) reveals that the difference is statistically significant.

We hence claim that the system benefits from the viscosity in terms of stability but the dropping viscosity induces the instability. The experimental results are comparable to the theoretical results obtained with a robot-robot configuration. In the region having a large dropping viscosity, the system is prone to be unstable.

3.2 | Experimental evaluation within in a human-robot context

Since the model for the theoretical analysis does not represent a human dynamics (whose model is not precisely known), the stability

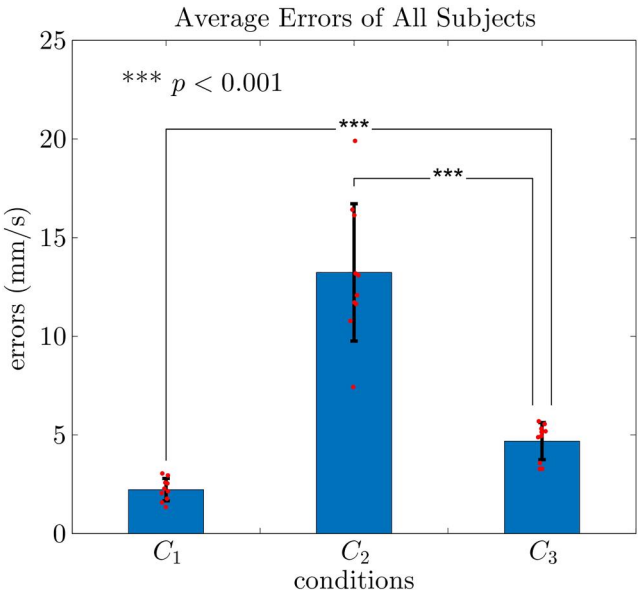

FIGURE 8 Average errors of all ten subjects under $C_1 - C_3$

condition is not appropriate for the practical controller tuning. However, in the current experiment, we have assumed the viscosity parameters in Section 3.1 unchanged. Besides, we add a first-order low pass filter with $\tau = 1s$ or $2s$.

The experiment protocol keeps the same as in Section 3.1. Specifically, we add four new conditions. $C_4 - C_6$ corresponds to $C_1 - C_3$, but with an additional viscosity filter ($\tau = 1s$). C_7 corresponds to C_2, with $\tau = 2s$. The conditions are listed in Table 1.

Figure 9 displays the velocity norm w.r.t time under $C_4 - C_7$ for the same subject in Figure 7. Under C_4 and C_6, the subject has similar performance as under C_1 and C_3. Under C_5 and C_7, the subject now has the ability to stabilise the velocity at v_d, compared with the unstable performance under C_2.

This observed behaviour is typical for all 10 subjects. Figure 10 is the RMS of velocity errors and the corresponding standard deviation under $C_1 - C_7$ (results under $C_1 - C_3$ reproduced from Figure 8). Conditions are organised based on their viscosity regions for better comparison.

The Student's t-test is also conducted. The RMS error under C_1 ($\mu = 2.2$, $\sigma = 0.57$, unit: mm/s, hereinafter the same) is close to that under C_4 ($\mu = 2.2$, $\sigma = 0.73$), evidenced by the statistically insignificant difference ($p = 0.86$). Similarly, the RMS error under C_3 ($\mu = 4.7$, $\sigma = 0.94$) is close to that under C_6 ($\mu = 4.2$, $\sigma = 1.0$) with $p = 0.25$. Therefore, we conclude that an additional viscosity coefficient filter does not degenerate the performance of the original stable areas, which was expected as the viscosity is supposed to be constant ($\alpha = 0$).

As to the RMS errors under C_2 with $\tau = 0s$ ($\mu = 13$, $\sigma = 3.5$), under C_5 with $\tau = 1s$ ($\mu = 4.2$, $\sigma = 1.1$) and under C_7 with $\tau = 2s$ ($\mu = 3.0$, $\sigma = 0.65$), due to the added filter, the values become drastically smaller, evidenced by statistically significant differences of p-values (9.5×10^{-6} for C_2 V.S. C_5 and 5.2×10^{-4} for C_5 V.S. C_7).

These observations are comparable to what was theoretically established for a robot-robot configuration: adding a filter with τ large enough leads to a locally asymptotically stable coupled system.

4 | CONCLUSION

This paper discusses about the variable viscosity control in the context of co-manipulation. The viscosity coefficient decreases as a function of velocity. An instability problem which has not been reported in literature, was theoretically shown using an robotics model and experimentally evidenced through human-robot experiments. We propose to add a secondary dynamics to slow down the viscosity variation. This proposition is supported by a theoretical analysis within the robotics context, while human-robot experiments show its practical efficiency in real applications.

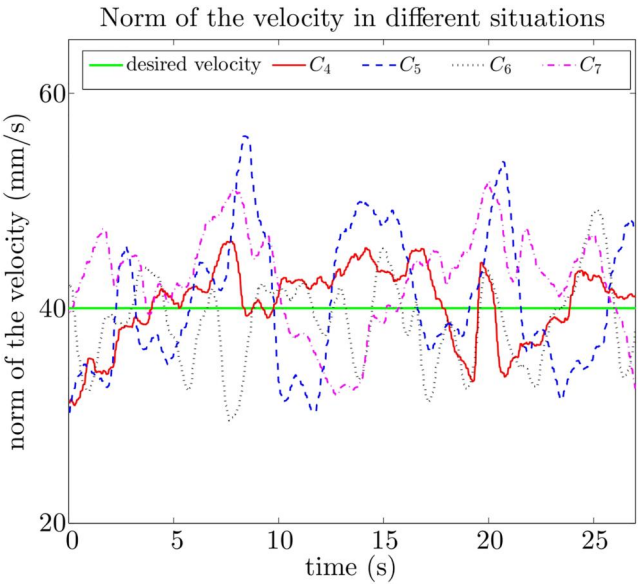

FIGURE 9 The velocity performance of a random subject under Conditions $C_4 - C_7$

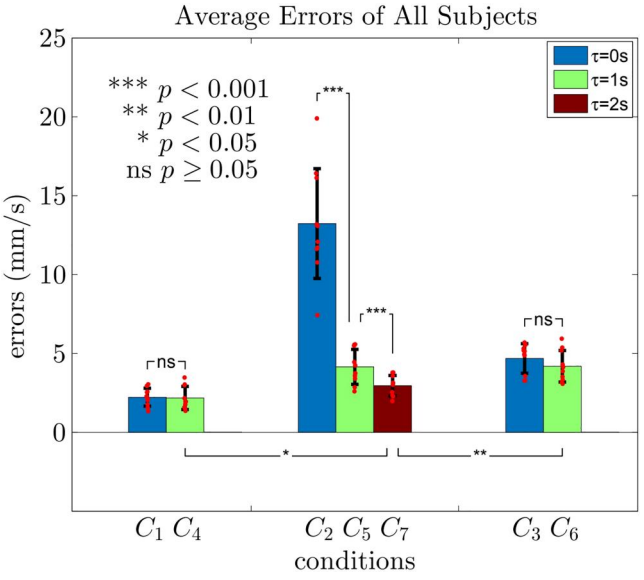

FIGURE 10 The average errors of all 10 subjects under $C_1 - C_7$

TABLE 1 The seven experimental conditions

Conditions	High viscosity coefficient (stable area)	Medium viscosity coefficient (unstable area)	Low viscosity coefficient (stable area)
No filter $\tau = 0s$	C_1	C_2	C_3
Filter $\tau = 1s$	C_4	C_5	C_6
Filter $\tau = 2s$	NA	C_7	NA

We study the instability problem of the variable viscosity control in the context of co-manipulation. Unlike tele-manipulated surgical robotic systems such as the da Vinci robot where the slave robotic arms mimic exactly the surgeon's motion, in co-manipulated robotic surgery, the involvement of human user makes the whole system dynamics different from the dynamics of the master/slave robotic system. For this reason, in the future work, more commercial co-operative robots with different mechanical structure such as Franka Emika Panda, Kuka iiwa, etc., shall replace Achilles as the co-manipulator to provide more solid experimental validation. In addition, we shall design more complicated human robot co-manipulation tasks such as following a given trajectory, virtual fixture guidance,[23] etc. to further verify the controller stability in the co-manipulated surgery.

ACKNOWLEDGEMENTS

This work was supported in part by the project FLUOROMIS funded by French FUI and by French state funds managed by the ANR within the Investissements d'Avenir programme (Labex CAMI) under reference ANR-11-LABX-0004.

CONFLICT OF INTEREST

The authors state explicitly that there are no conflict of interest in connection with this article.

DATA AVAILABILITY STATEMENT

The data that support the findings of this study are available from the corresponding author upon reasonable request.

ORCID

Lin Dong https://orcid.org/0000-0001-7141-0355

REFERENCES

1. Su H, Qi W, Hu Y, Karimi HR, Ferrigno G, De Momi E. An incremental learning framework for human-like redundancy optimization of anthropomorphic manipulators. *IEEE Trans Ind Inf*. 2020.
2. Lamy X, Colledani F, Geffard F, Measson Y, Morel G. Robotic skin structure and performances for industrial robot comanipulation. *IEEE*. 2009:427-432. https://doi.org/10.1109/aim.2009.5229975
3. Dong L, Morel G. Robust trocar detection and localization during robot-assisted endoscopic surgery. *IEEE*. 2016:4109-4114.
4. Su H, Hu Y, Karimi HR, Knoll A, Ferrigno G, De Momi E. Improved recurrent neural network-based manipulator control with remote center of motion constraints: experimental results. *Neural Network*. 2020;131:291-299. https://doi.org/10.1016/j.neunet.2020.07.033
5. Su H, Mariani A, Ovur SE, Menciassi A, Ferrigno G, De Momi E. Toward teaching by demonstration for robot-assisted minimally invasive surgery. *IEEE Trans Autom Sci Eng*. 2021;18(2):484-494. https://doi.org/10.1109/tase.2020.3045655
6. Moustris GP, Hiridis SC, Deliparaschos KM, Konstantinidis KM. Evolution of autonomous and semi-autonomous robotic surgical systems: a review of the literature. *Int J Med robotics Comput Assisted Surg*. 2011;7(4):375-392. https://doi.org/10.1002/rcs.408
7. Dong L, Morel G. Robust trocar identification and its application in robotic minimally invasive surgery. *Int J Med Robotics Comput Assisted Surg*. 2022:e2392.
8. Alanee S, El-Zawahry A. Robotic-assisted partial cystectomy for muscle invasive bladder cancer: contemporary experience. *Int J Med Robotics Comput Assisted Surg*. e2390.
9. Qi W, Su H, Aliverti A. A smartphone-based adaptive recognition and real-time monitoring system for human activities. *IEEE Transactions on Human-Machine Systems*. 2020;50(5):414-423. https://doi.org/10.1109/thms.2020.2984181
10. Peternel L, Tsagarakis N, Caldwell D, Ajoudani A. Adaptation of robot physical behaviour to human fatigue in human-robot co-manipulation. *IEEE*. 2016:489-494. https://doi.org/10.1109/humanoids.2016.7803320
11. Roveda L, Maskani J, Franceschi P, et al. Model-based reinforcement learning variable impedance control for human-robot collaboration. *J Intell Rob Syst*. 2020;100(2):417-433. https://doi.org/10.1007/s10846-020-01183-3
12. Huang J, Pham DT, Wang Y, et al. A case study in human–robot collaboration in the disassembly of press-fitted components. *Proc IME B J Eng Manufact*. 2020;234(3):654-664. https://doi.org/10.1177/0954405419883060
13. Beretta E, Nessi F, Ferrigno G, et al. Enhanced torque-based impedance control to assist brain targeting during open-skull neurosurgery: a feasibility study. *Int J Med Robotics Comput Assisted Surg*. 2016;12(3):326-341. https://doi.org/10.1002/rcs.1690
14. Wu Z, Chen Y, Geng Y, Wang X, Xuan B. Model-free robust adaptive integral sliding mode impedance control of knee-ankle-toe active transfemoral prosthesis. *Int J Med Robotics Comput Assisted Surg*. 2022;18(3):e2378. https://doi.org/10.1002/rcs.2378
15. Bowyer SA, Davies BL, Baena yFR. Active constraints/virtual fixtures: a survey. *IEEE Trans Robot*. 2013;30(1):138-157. https://doi.org/10.1109/tro.2013.2283410
16. Ikeura R, Inooka H. Variable impedance control of a robot for cooperation with a human. *IEEE*. Vol 3;1995:3097-3102.
17. Ikeura R, Moriguchi T, Mizutani K. Optimal variable impedance control for a robot and its application to lifting an object with a human. *IEEE*; 2002:500-505.
18. Flash T, Hogan N. The coordination of arm movements: an experimentally confirmed mathematical model. *J Neurosci*. 1985;5(7):1688-1703. https://doi.org/10.1523/jneurosci.05-07-01688.1985
19. Huo Y, Li X, Zhang X, Sun D. Intention-driven variable impedance control for physical human-robot interaction. *IEEE*. 2021:1220-1225. https://doi.org/10.1109/aim46487.2021.9517438
20. Erden MS, Marić B. Assisting manual welding with robot. *Robotics Computer-Integrated Manuf*. 2011;27(4):818-828. https://doi.org/10.1016/j.rcim.2011.01.003
21. Morel G, Dong L, Richer F, Perrin N, Vidal C, Bardou B. *Method and device to assist with the operation of an instrument*. 2020. US Patent 10,582,977.
22. Dupont PE. Avoiding stick-slip through PD control. *IEEE Trans Automat Control*. 1994;39(5):1094-1097. https://doi.org/10.1109/9.284901
23. Gruijthuijsen C, Dong L, Morel G, Vander Poorten E. Leveraging the fulcrum point in robotic minimally invasive surgery. *IEEE Rob Autom Lett*. 2018;3(3):2071-2078. https://doi.org/10.1109/lra.2018.2809495

How to cite this article: Dong L, Perrin N, Richer F, Roby-Brami A, Morel G. The stability investigation of variable viscosity control in the human-robot interaction. *Int J Med Robot*. 2022;18(5):e2416. https://doi.org/10.1002/rcs.2416